Applied Surface Science 257 (2010) 1684–1691

Contents lists available at ScienceDirect

Applied Surface Science

journal homepage: www.elsevier.com/locate/apsusc

Surface studies on bimetallic thiocyanate ligand based single crystals of $MnHg(SCN)_4$, $CdHg(SCN)_4$ and $ZnCd(SCN)_4$

T. Rajesh Kumar[a], R. Jeyasekaran[a], S.M. Ravi Kumar[b], M. Vimalan[c], P. Sagayaraj[a,*]

[a] Department of Physics, Loyola College, Chennai 600 034, India
[b] Department of Physics, Govt. Arts College, Thiruvannamalai 606 603, India
[c] Physics Research Center, S.T. Hindu College, Nagercoil 629 002, India

ARTICLE INFO

Article history:
Received 21 June 2010
Received in revised form 28 August 2010
Accepted 30 August 2010
Available online 9 September 2010

Keywords:
Optical microscopy
Organometallic
Laser damage threshold
Atomic force microscopy
SEM
Etching

ABSTRACT

Bimetallic SCN ligand based single crystals of manganese mercury thiocyanate (MMTC), cadmium mercury thiocyanate (CMTC) and zinc cadmium thiocyanate (ZCTC) are grown by slow solvent evaporation technique. The growth mechanism and surface features are investigated by optical microscopic techniques such as scanning electron microscopy (SEM) and atomic force microscopy (AFM). The laser induced surface damage measurements were carried out using a Q-switched Nd:YAG laser at 1064 nm with laser beam of 1.0 Hz and pulse duration 25 ps. The laser damage threshold values of MMTC, CMTC and ZCTC are found to be 15.9, 22.9 and 19.7 GW/cm^2, respectively. The SEM analysis of MMTC reveals the formation of elongated dendrite growth pattern caused by the fluctuations of Mn and Hg metal ligands when thiocyanate (SCN) bridges them. The etching study indicates the occurrence of different types of etch pit patterns like terraced triangles, pillars, pyramids and rods. The AFM images confirm the formation of three major hillocks with cavities in MMTC. The measured roughness values for CMTC crystal are very much lower than that of MMTC.

1. Introduction

Second order nonlinear optical (SONLO) materials which are capable of efficient frequency conversion of infrared laser radiation to visible or ultraviolet (UV) wavelengths are of considerable interest for many applications such as high-density optical data storage, medical diagnosis, photolithography, underwater communication and laser displays [1–6]. Materials with large second order optical nonlinearities, transparency at required wavelengths and stable physicochemical performance are needed to realize many of these applications. Among the different varieties of NLO materials investigated, the organometallics are gaining rapid interest due to their interesting and intriguing properties. Organometallic compounds (which contain at least one direct M–C bond between metal and organic ligands) and coordination compounds (in which the metal and the ligands are connected through M–O, M–N, M–S or M–P bonds) are the compounds, which combine the features of both inorganic and organic compounds [7]. Organometallic and coordination compounds offer a variety of molecular structures by changing the metals, ligands, coordination numbers and so on. This diversity of molecular structure gives an opportunity to tune the electronic properties of the molecules, and hence to exploit the linear and nonlinear optical properties [8–15].

Continuous research for the past two decades on different types of organometallic crystals formed with organic ligands like: urea, thiourea, allylthiourea, thio semi-carbozide and thiocyanate, confirm the NLO activity in these materials [7,16–18]. Among them, the crystals formed with thiocyanate (SCN) ligand show a relatively higher SHG effect than the crystals formed with the other organic ligands. Particularly, the bimetallic thiocyanate complexes with $AB(SCN)_4$ (where, A = Mn, Cd and Zn; B = Hg and Cd) structure type; $MnHg(SCN)_4$ (MMTC), $CdHg(SCN)_4$ (CMTC) and $ZnCd(SCN)_4$ (ZCTC) possess favourable properties to become candidate materials for SHG devices [19–22].

In metal thiocyanate complexes, the thiocyanate (SCN) plays a crucial role in combining the versatile ambidentate ligand with two donor atoms. The modes of metal coordination with thiocyanates are best understood in terms of the Hard–Soft Acid–Base (HSAB) concept developed by Pearson, Balarew and Duhlew [23,24]. In accordance with the hard–soft acid–base concept, the S atom of the SCN^- ligand, being a soft base, preferentially coordinates to the soft acid whereas; the N atom, being a hard base, preferentially coordinates to the hard acid. Bimetallic thiocyanates of MMTC, CMTC and ZCTC consist of two kinds of slightly flattened tetrahedral: AN_4 and BS_4. The most striking features are; the –N=C=S– bridges which connect the center atoms of the infinite three dimensional –A–N=C=S–B– networks. The metal ligand bonding

* Corresponding author at: Department of Physics, Loyola College, Sterling Road, Chennai, Tamil Nadu 600 034, India. Tel.: +91 44 28178200; fax: +91 44 28175566.
E-mail address: psagayaraj@hotmail.com (P. Sagayaraj).

0169-4332/$ – see front matter © 2010 Elsevier B.V. All rights reserved.
doi:10.1016/j.apsusc.2010.08.123

in organometallics gives rise to the large macroscopic nonlinearities and excellent physicochemical stabilities due to the transfer of electron density between the metal atoms and the conjugated ligand systems [25].

Based on these considerations, three coordination complex materials, namely, MMTC, CMTC and ZCTC have been investigated in this work.

Manganese mercury thiocyanate (MMTC) crystal belongs to the tetragonal crystallographic system with space group $I\bar{4}$ [26]. Geng et al. have investigated the growth mechanism of MMTC crystal by atomic force microscopy (AFM) and concluded that the crystal surface grows by 2D nucleation mechanism [27]. The reported powder SHG efficiency of MMTC is higher than that of CMTC and ZCTC [20]. Furthermore, during crystal processing, MMTC is much easier to process compared with CMTC which shows that MMTC crystal has a high mechanical strength for device processing [25].

The growth of CMTC crystals was first studied by Masakatsu Lizuka and Toshio Sudo in 1968, by temperature lowering method [28]. In the initial stages, due to severe growth difficulties, poor crystal size and inadequate crystal quality, the application of CMTC as a nonlinear optical crystal was neglected for many years. Von Hundelshausen had grown CMTC crystal and studied their electro-optic effect and dielectric properties [29]. Yuan et al. have reported the growth of large size and improved optical quality single crystals of CMTC from mixture solvents of water and NaCl (or KCl) by temperature lowering method [22]. By frequency doubling with an 809 nm laser diode, violet light at 404.5 nm has been obtained in CMTC [30]. There are reports on the growth mechanism of CMTC crystal by atomic force microscopy (AFM) [31].

ZCTC belongs to tetragonal system, space group $I\bar{4}$ with $a = 11.135(2)$ Å, $c = 4.3760(10$Å, $V = 542.6(2)$ Å^3, $Z = 2$, $D_c = 2.510$ g/cm^3. High optical quality ZCTC single crystals were grown by Wang et al. [1]. Growth mechanism and surface morphologies of ZCTC crystals grown at various conditions have been investigated by high resolution atomic force microscopy. The morphology of {1 0 0} face of the ZCTC crystal before and after their growth at (30 ± 0.05 °C) was observed. Highlands formed by chains of small growth hillocks generated by spiral dislocation sources and small cavities adjacent to the hillocks are observed at this grown surface [31].

Though the growth of MMTC, CMTC and ZCTC crystals have been achieved by the crystal growers, there are still challenges pertaining to the growth of large size single crystals free from defects. For crystal growers, an in-depth understanding about the growth mechanism and surface morphology of crystals is needed, which can do much help in accelerating the growth rate, enhancing the crystal quality and thereby expediting the crystal development. Unfortunately, it is somewhat difficult to grow these crystals into high quality materials of useful size, which has limited their applications to a certain extent. Therefore, it is very important to investigate the growth mechanism, morphologies and defects by different techniques. In this article, the surface features on the grown crystals of MMTC, CMTC and ZCTC are investigated by employing surface laser damage threshold (LDT), scanning electron microscopy (SEM), etching and atomic force microscopy (AFM) studies.

2. Experimental

2.1. Crystal growth

High purity (E-Merck, AR grade) starting materials of ammonium thiocyanate (NH_4SCN), mercury chloride ($HgCl_2$), cadmium chloride ($CdCl_2$), zinc chloride ($ZnCl_2$) and manganese chloride ($MnCl_2$) were purchased. Manganese mercury thiocyanate ($MnHg(SCN)_4$), cadmium mercury thiocyanate ($CdHg(SCN)_4$) and zinc cadmium thiocyanate ($ZnCd(SCN)_4$) were synthesized using appropriate solvent (water for MMTC, water with ethanol for CMTC and water with acetone for ZCTC). The following reaction formulae were used to synthesis the compounds:

(i) for manganese mercury thiocyanate,

$$4NH_4SCN + MnCl_2 + HgCl_2 \rightarrow MnHg(SCN)_4 + 4NH_4Cl$$

(ii) for cadmium mercury thiocyanate,

$$4NH_4SCN + CdCl_2 + HgCl_2 \rightarrow CdHg(SCN)_4 + 4NH_4Cl$$

(iii) for zinc cadmium thiocyanate,

$$4NH_4SCN + ZnCl_2 + CdCl_2 \rightarrow ZnHg(SCN)_4 + 4NH_4Cl$$

To ensure high purity, the materials were purified by successive recrystallization (typically 3–4 times) in Millipore water.

The growth of bulk size single crystals of MMTC, CMTC and ZCTC was carried out in a constant temperature bath with an accuracy of ±0.01 °C by slow solvent evaporation method adopting the same experimental procedure reported already by our research group and Wang and co-workers [1,20,21].

Recrystallized salt of MMTC was taken and dissolved in water according to the solubility data. The solution was constantly stirred for 24 h using magnetic stirrer to overcome the concentration gradient in the crystallizer. The saturated solution was taken in a crystallizing vessel and covered with a perforated sheet to facilitate slow evaporation of the solvent at room temperature. The solution gradually attained supersaturation due to evaporation which resulted in nucleation followed by the growth of crystals. Single crystals with perfect external shape were obtained by spontaneous nucleation within a period of 5–10 days. Good quality crystals, free from macro defects were chosen as seeds to carry out further growth experiments. The seed crystals were kept suspended in to the reactant mother solution kept in the beaker. The solvent was allowed to evaporate at a constant temperature of 305 K by covering the vessel with a perforated lid. From the mother solution of pH = 2.8, a relatively large size crystal of dimension 14 mm × 12 mm × 4 mm was successfully grown in a period of 50–60 days.

The growth of CMTC crystal is the effective stacking of growth units $[Hg(SCN)_4]^{2-}$ and Cd^{2+} ions. The growth of crystal was carried out by slow solvent evaporation of the reaction mother solution at room temperature. In the first stage, high purity CMTC was synthesized and the synthesized product was used for further growth experiments. CMTC showed a relatively high solubility in the mixture of water and ethanol (1:1), the homogenized solution was covered with air-tight sheet, which controls the evaporation of ethanol from the mixed solution and then kept in a constant temperature bath. CMTC crystals of dimension up to 10 mm × 9 mm × 3 mm were obtained in a period of 20–30 days.

The synthesized product of ZCTC was purified by recrystallization and dissolved in mixed solvent of acetone and water (4:1). In accordance with the solubility data, saturated solution of 200 ml of ZCTC was prepared. The prepared solution of ZCTC was allowed to evaporate at room temperature (303 K). In a period of 5–7 days, tiny, transparent and needle shape crystals were obtained. Among them, defect free seed crystals were taken and kept immersed into the reactant mother solution. Within a period of 15–20 days ZCTC crystals of sizes up to 7 mm × 5 mm × 3 mm were formed. The crystals appear colourless and are non-hygroscopic in nature.

In order to determine the laser induced surface damage threshold of crystals of MMTC, CMTC and ZCTC, a Q-switched Nd:YAG laser

(1064 nm, 25 ps, 1.0 Hz) was used. The laser beam was focused using a focal spot size was nearly 130 μm ($1/e^2$ radius). Power supply serves to adjust the input intensity to the required level and measurement was carried out at phase matching conditions. A photo diode was used to identify beam and sufficient time was allowed to stabilize the output power of laser. The crystals were placed on a sample holder and kept slightly away from the focal spot of the beam to avoid any possible damage. The scattered second harmonic signal from the crystal was collected using a collecting lens and was monitored using a monochromator and oscilloscope. The occurrence of damage was monitored on the oscilloscope and irrespective of whether the damage had occurred or not the sample was moved to a new site. The separation of two sites was kept at least seven times the spot size on the crystal surface. Thus, any kind of cumulative effect was completely avoided. This facilitated accurate measurement, eliminating the possibility of the sample getting damaged at laser radiation fluence [32,33]. It is known that SHG output is increased on increasing the incident energy and reaches a maximum until damage occurs and decreases after damage for further increases of incident energy. The corresponding energy for maximum SHG output was taken for calculation.

$$M^2 = \frac{\theta_0 \pi D_0}{4\lambda}$$

where M is the laser quality and θ_0 is the beam divergence (0.5 m rad). The diameter of the spot and the surface damage threshold of the crystals were calculated using the equations.

$$d = \frac{M^2 f 4\lambda}{\pi D_0}$$

$$P = \frac{E}{\tau \pi r^2}$$

where d is diameter of the spot (mm), τ is the pulse width (ps), f is the focal length, λ is 1064 nm, D_0 is the beam divergence length (1 cm), r is the radius of the spot (mm) and E is the energy (mJ).

The surface morphologies, smoothness and defects of the as grown crystals of MMTC, CMTC and ZCTC were investigated using JEOL/EO-JSM-5610 and Hitachi Scanning Electron Microscope Model S-4200 operated at 25 kV. For etching study, several etchants were used on trial and error basis and finally water and ethanol were chosen as the most suitable etchants for the samples of MMTC, CMTC and ZCTC. The experiments were performed at room temperature. The capacity of revealing etch pits by a solvent on different faces also depends on the crystallographic orientation [34]. Hence, thin plates of typical thickness (2–3 mm), parallel to the most prominent faces of (1 1 0), (1 1 0) and (1 0 0) for MMTC, CMTC and ZCTC crystals, respectively were cut out from the as grown crystal using a wet thread. In order to etch the sample, the chosen crystal face was carefully dipped in the selected etchant for a typical period ranging from 10 to 50 s at room temperature and then wiped with dry filter paper. The etch pits patterns were photographed with an OLYMPUS BX51 microscope. The surface characteristics were studied with the aid of a CSPM 4000 atomic force microscope (AFM) and the AFM images were analyzed with SPM console software.

3. Results and discussion

3.1. Laser damage threshold measurement

The laser damage threshold is an important factor for NLO materials. The laser damage threshold values of MMTC, CMTC and ZCTC are found to be 15.9, 22.9 and 19.7 GW/cm^2, respectively. The laser induced surface damage threshold of a few well known NLO crystals are presented in Table 1 for comparison. Usually, the organic crystals show very high damage threshold value than the inorganic counterparts and the modification in the laser induced threshold values occur when inorganic elements are combined with organic derivatives/ligands [35]. The present study is of great interest to find out the influence of combining an organic SCN ligand with metals and find out the modification in the laser induced damage and thereby prescribe the maximum permissible laser power for the organometallic crystals developed. It is clearly evident from table that the damage threshold values of MMTC, CMTC and ZCTC are much higher than few well known inorganic crystals like BBO, LBO, KTP and KDP and comparable to few organic crystals [7,35–38]. The study thus confirms the high resistance of the SCN ligand based organometallic crystals to optical damage and proves the suitability of the materials for high power laser related applications. Since organic materials have moderate environmental stability, low mechanical strength and a limited temperature of operation, the organometallic NLO crystals investigated in this work provide better options and variety in the field of nonlinear optics.

Table 1
Comparison of laser damage threshold of few well known NLO crystals.

Crystal	Laser damage threshold (GW/cm^2)
MMTC	15.9 (1064 nm, 10 ns)
CMTC	22.9 (1064 nm, 10 ns)
ZCTC	19.7 (1064 nm, 10 ns)
LBO	>0.6 (1064 nm, 18 ns, 10 Hz)
KB5	>0.085 (1064 nm, 12 ns, 10 Hz)
KDP	14.4 (1064 nm, 12 ns, 30 μm)
ADP	6.4 (1064 nm, 12 ns, 30 μm)
KTP	1.5–2.2 (1064 nm, 11 ns, 2 Hz)
LAP	10–13 (1064 nm, 1 ns)
Urea	5 (1064 nm, 10 ns)
POM	2 (1064 nm, 20 ns)

Fig. 1a–c shows the magnified images of the damaged surface of the MMTC, CMTC and ZCTC crystals. At the damage spot, one can see various features like melting and solidification in the form of circular blobs adjacent to the damage site, highly reflecting regions due to cleavage, ablation of material and cracking. The morphology of the damaged patterns reveals the nature of damage and their possible origins [39]. When the damage is caused by the dielectric break down, there will be a clear symmetry of the resultant pattern. At the same time, when the damage is predominantly by thermal decomposition, the patterns observed do not show any symmetry and are surrounded by a circular halo. However, these are only indicative of the dominant mechanism and the actual process of laser damage is a complex interplay of various contributing mechanisms. Other dominating factors include experimental geometry, specific properties of the material, pulse width and wavelength of the laser radiation used [35]. It is clear from the image (Fig. 1a) of MMTC crystal that the damage pattern does not show any symmetry and are often surrounded by circular halo and thus damage is predominantly due to thermal decomposition. Further, the damage pattern is highly local and had no major cracks or fragmentation. In the case of CMTC, the damage pattern (Fig. 1b) is not localized but contains small cracks spread out on the surface. From the damage threshold data, it can be concluded that CMTC has good resistance towards the laser induced thermal radiation or dielectric breakdown effect. On the other hand, the effect of laser radiation on ZCTC crystal reveals that damage pattern (Fig. 1c) is highly localized and does not show any cracks on the surface. Thus it concluded that among the three crystals, CMTC has shown better damage resistance towards the laser radiation with high value of 22.9 GW/cm^2.

3.2. Scanning electron microscopy

The as grown crystals with well defined planes and of smooth surface were selected for the SEM analysis and no polishing was

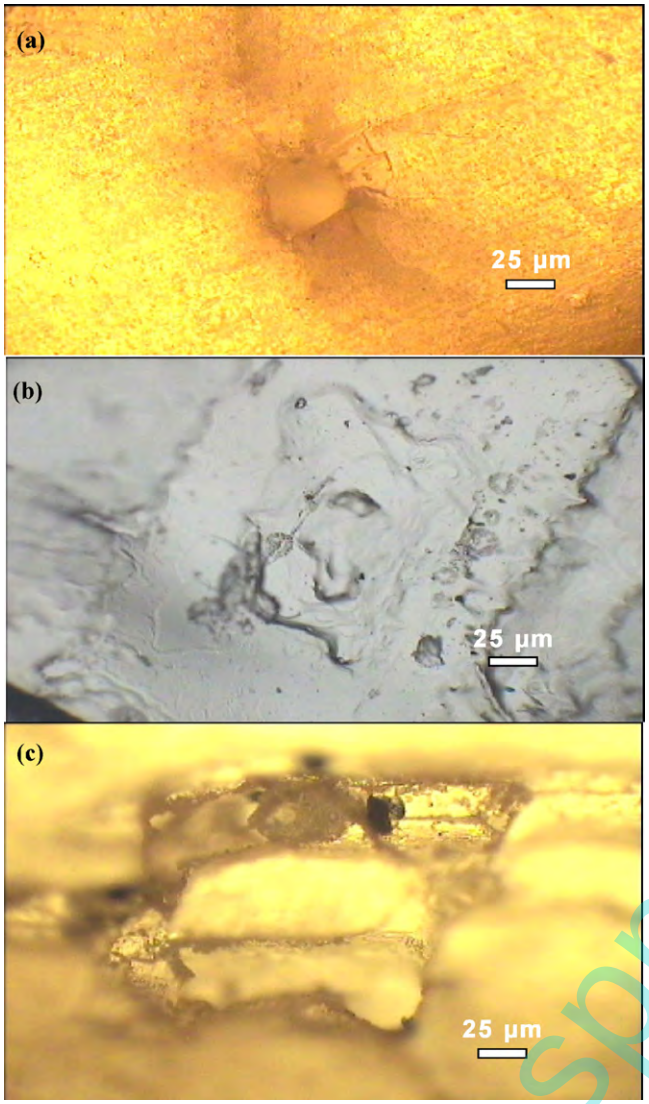

Fig. 1. Optical micrograph of laser induced surface damage of (a) MMTC, (b) CMTC and (c) ZCTC.

done. It is clear from the SEM micrographs of MMTC (Fig. 2a) that crystal surfaces contains voids of irregular size and dendrites like growth pattern of microcrystals. The presence of valley and cracks are predominantly seen on the surface of the crystal. It is believed that the MMTC is prone to such defects unless the growth parameters like temperature and pH is carefully optimized. The dendrites growth like pattern of small microcrystallites over the crystal surface is exclusively due to multi-nucleation as the results of significant amount of unreacted monomer concentration in the mother solution. With increased magnification (Fig. 2b), the elongated dendrite growth patterns are clearly visible and these patterns are possibly caused by the fluctuation of Mn and Hg metal ligands when SCN bridges them to form the three dimensional network [25].

In the case of CMTC crystal, a dramatic change in its surface morphology is observed as compared to MMTC. From the SEM micrographs shown in Fig. 3a, it is clear that the crystal possesses almost smooth surface and free from cracks and large size voids. However, very few microcrystals are seen on the surface when viewed with enhanced magnification (Fig. 3b). The effective control over the growth parameters is attributed to the improvement in the crystal's surface quality. The occurrence of multi-nucleation encountered during the growth of MMTC is avoided to a larger extent in the case of CMTC. Hence, it is clear that CMTC crystals have improved surface morphology when compared with MMTC crystals.

The SEM micrograph taken on the selected planes of ZCTC, Fig. 4a and b shows that the crystal surface on the whole appear smooth but there are also few isolated islands and minute crystallites over the surface. Thus the SEM analysis indicates that CMTC and ZCTC crystals possess relatively smooth surfaces and free from major defects when compared to MMTC crystal.

3.3. Etching study

The etching study reveals the structural perfection and growth features of the grown single crystal. The chemical etching studies were carried out on the as grown single crystals of MMTC, CMTC and ZCTC to study the symmetry of the crystal from the shape of etch pits and the distribution of structural defects in the grown crystals [34]. The etching firstly happens and develops at the dislocation outcrop on the surface of the crystal. If proper etchant is used, under the appropriate temperature and time of etching, the corresponding dislocation etch pits can be shown on the surface of the polished sample. First, the crystal sample was completely immersed in the etchant and then etched sample was cleaned using a tissue paper and the etch patterns were observed using an optical microscope. Fast etchants like water and ethanol could produce well defined etch pits on the surfaces.

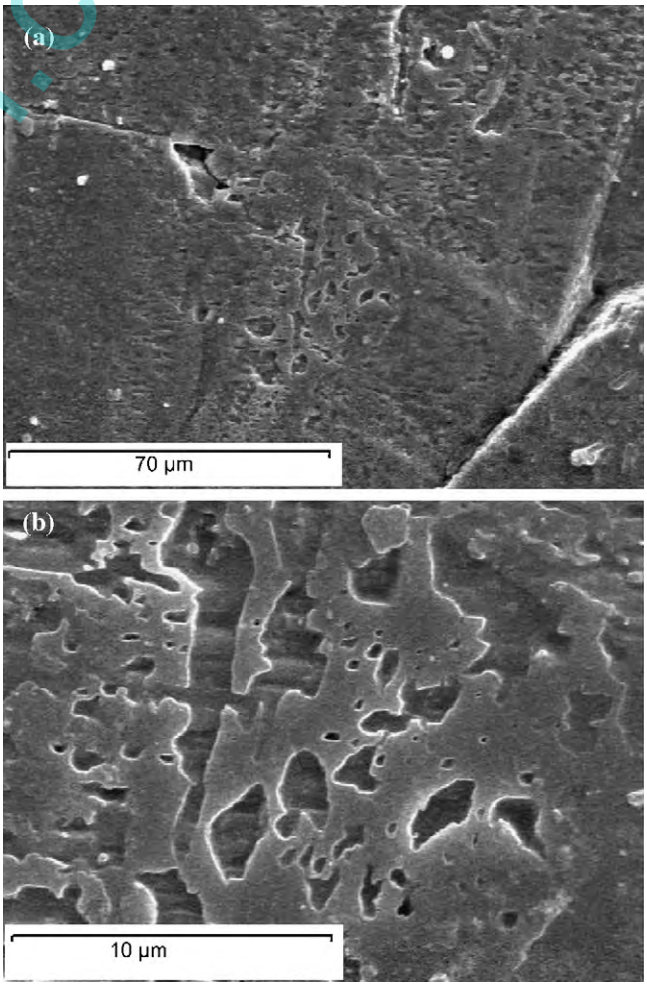

Fig. 2. SEM pictures of MMTC (a) the surface containing voids and (b) elongated dendrites growth patterns are seen.

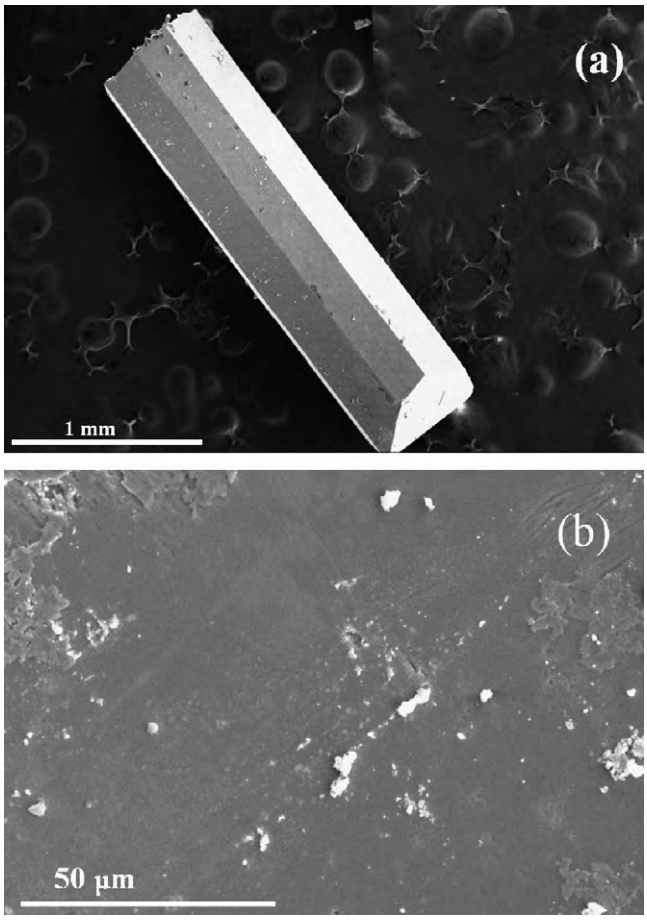

Fig. 3. SEM pictures of CMTC (a) smooth surface and (b) microcrystals on the surface.

The selective dissolution of (1 1 0) plane of the MMTC using water as the etchant reveals the lattice defects of the sample. Fig. 5a shows the surface of the etched MMTC, where a bulk void could be seen on the surface, which was due to the trapping of air molecule during the solidification of the material. The etching pattern for MMTC agrees well with the AFM images taken for the sample and thus confirming the formation of dislocation on the grown crystal. When MMTC is etched with ethanol, tiny rod like pattern (Fig. 5b) is observed and also the lines like etch pits are clearly observed due to grain boundary. In the case of CMTC crystals etched with water, in (1 1 0) orientation, triangular (positive) etch pits were obtained for an etching time of 50 s (Fig. 6a). However, when ethanol was used as an etchant, shadowed pillar like etch pits pattern (Fig. 6b) were obtained at a relatively low etching time (10 s). Fig. 7a shows the pyramidal etch pits obtained by etching ZCTC (1 0 0) surface in water for 50 s. Fig. 7b shows the etch pits obtained by etching ZCTC surface in ethanol for 10 s. The etch pits are terraced triangle in shape. It is well known that the time of etching is related to some extent to the occurrence and symmetry of different faces. It has been observed by several researchers that the size of the pattern increases with increase in etching time. In the present case also such similar trend has been noticed. Further, the patterns obtained were quite stable and did not degrade for several days.

3.4. Atomic force microscopy

Figs. 8–10 show the 100,000 nm × 10,000 nm image morphologies of MMTC, CMTC and ZCTC crystals on the (1 1 0), (1 1 0) and (1 0 0) face of respective sample. It is evident from the morphology of MMTC (Fig. 8) that the surface contains three major hillocks with cavities. There are also long highlands and such highlands are formed by chains of small growth hillocks with cavities. These features are probably caused by unequal growth at neighboring hollow channels. The formation of the unique screw dislocation, at the origin of which there exists a valley, is also shown in Fig. 8. It can be examined that the depth of the valley is about 123 nm. It is well known that a large number of peaks and valleys in an image significantly affect the average roughness (S_a) and root mean square (S_q) values [40]. Thus due to the presence of increased number of peaks and valleys, the estimated roughness values (S_a = 40.6 and S_q = 67.8 nm) are on the higher side for MMTC than that of CMTC and ZCTC. The AFM image (Fig. 9) for CMTC crystal indicates that the surface contains striations like pattern and the presence of strong peaks are ruled out. This is quite correct in the sense that the measured roughness values (S_a = 4.77 and S_q = 6.63 nm) are reduced at least one tenth than that of MMTC. It is evident from the image (Fig. 10) for ZCTC that the sample possesses cleavage steps and they are always imaged at the slopes of large growth hillocks generated by simple or complex dislocation sources. Between the steps there exists a tiny but long hole. The ten-point height (S_z), which is regarded as the difference in height between the average of the five highest peaks and the five lowest valley along the assessment length of the profile is found to be high (686 nm) for MMTC when compared to CMTC and ZCTC crystals. Surface skewness (S_{sk})

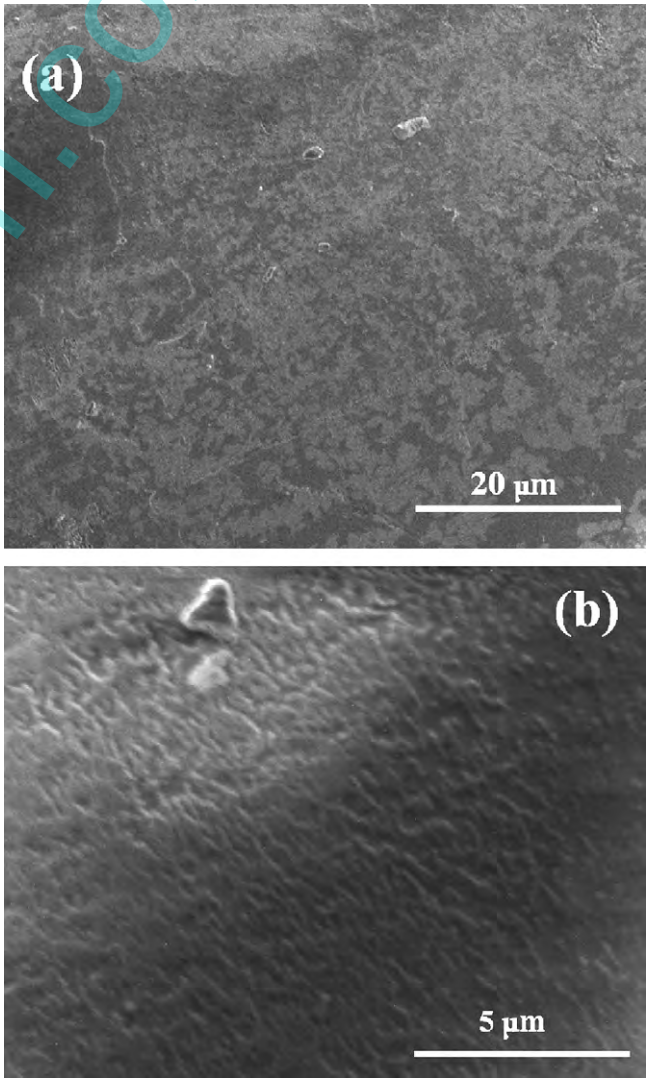

Fig. 4. SEM pictures of ZCTC showing the smooth surface.

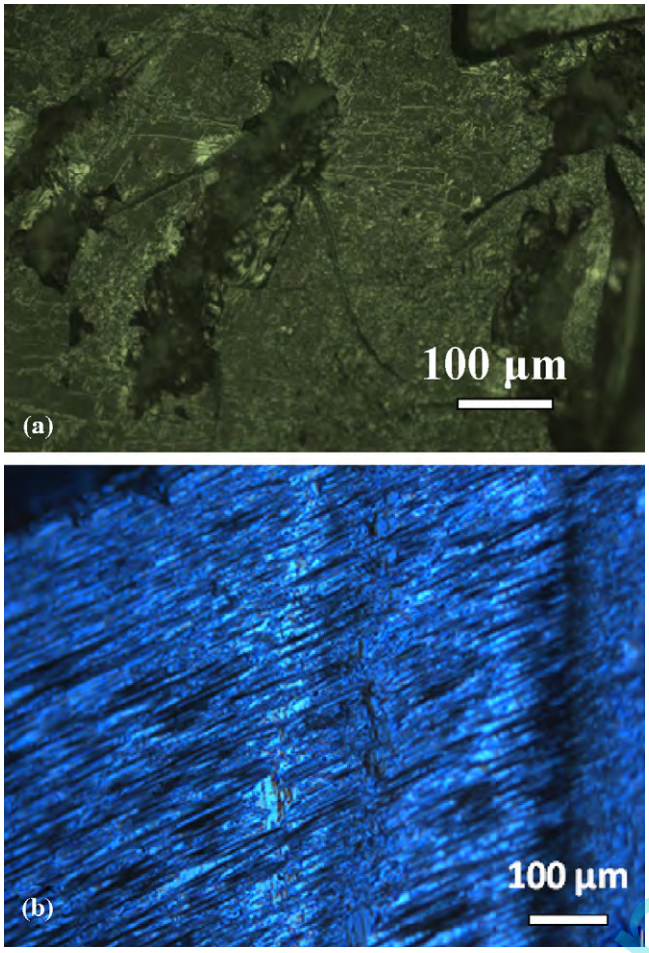

Fig. 5. Surface of MMTC etched by (a) water (50 s) and (b) ethanol (10 s).

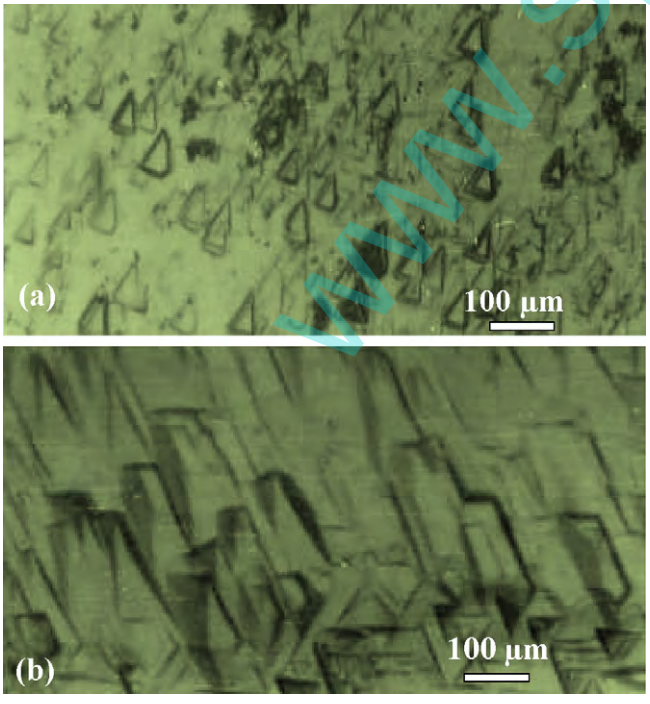

Fig. 6. Etch pits (25× magnification) on the surface of CMTC etched by (a) water (50 s) and (b) ethanol (10 s).

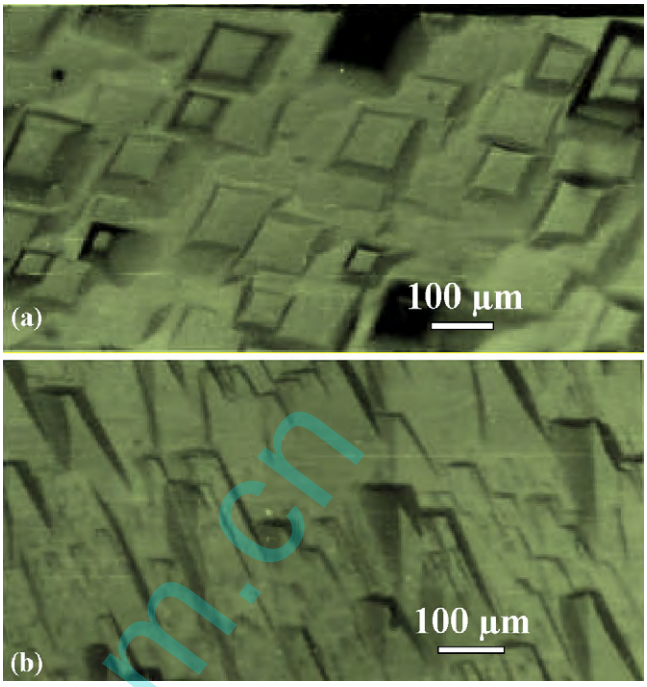

Fig. 7. Etch pits (25× magnification) on the surface of ZCTC etched by (a) water (50 s) and (b) ethanol (10 s).

values of MMTC (−0.79) and ZCTC (−0.482) were negative compared to CMTC which has positive value of 0.226. It has been reported that if the height distribution is asymmetrical and the surface has more peaks than valleys, the Skewness moment is positive, and if the surface is more planar and the valleys are predominant then the Skewness is negative [40].

Thus it is clear from the Skewness data shown in Table 2 that CMTC crystal surface possesses almost smooth surface, whereas, MMTC and ZCTC surfaces posses relatively large number of valleys. Similarly, another important surface parameter, namely, surface kurtosis (S_{ku}) is the measure of surface sharpness. If S_{ku} is smaller than 3, the surface is regarded as a perfectly flat one and if $S_{ku} > 3$, the surface is set to have more peaks than valleys. Thus, based on the data for S_{sk} and S_{ku} for the three samples it can be concluded that among the three crystals, the surface of CMTC is smoother than that of MMTC and ZCTC.

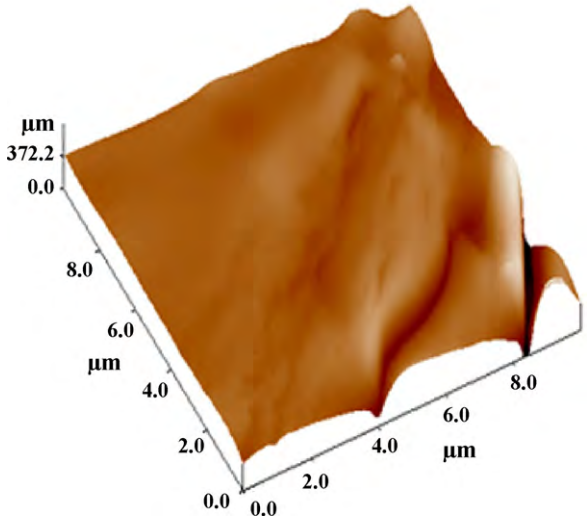

Fig. 8. AFM image of MMTC.

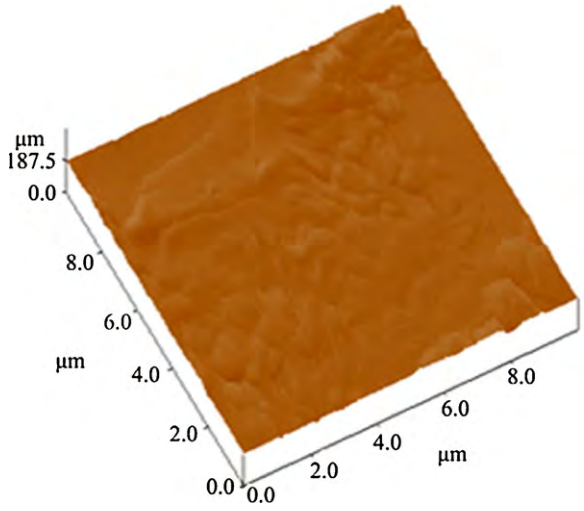

Fig. 9. AFM image of CMTC.

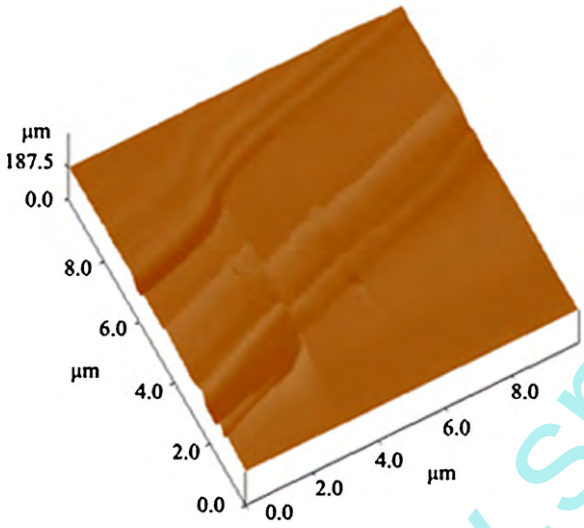

Fig. 10. AFM image of ZCTC.

Table 2
Different parameters of MMTC, CMTC and ZCTC measured by AFM.

Parameter	MMTC	CMTC	ZCTC
Roughness average (S_a) (nm)	40.6	4.77	5.49
Root mean square (S_q) (nm)	67.8	6.63	8.16
Surface skewness (S_{sk})	−0.79	0.226	−0.482
Surface kurtosis (S_{ku})	11.1	4.74	5.59
Ten-point height (S_z) (nm)	686	54.9	59.7
Density of summits (S_{ds}) (1/µm^2)	10.9	21.2	6.17
Fractal dimension	2.46	2.77	2.42

4. Conclusion

Single crystals of bimetallic thiocyanates of MMTC, CMTC and ZCTC were grown by solution method. The surface properties of the crystals were investigated by laser induced damage threshold, SEM, Etching and AFM and the results are discussed. The laser damage threshold measurement confirms the moderate damage resistance of the grown crystals and it is much better than some of the popular inorganic crystals. The SEM analysis shows the screw dislocation in MMTC crystal, further the study indicate that CMTC and ZCTC crystals possess relatively smooth surfaces when compared to MMTC. The etching study confirms the growth pattern and the formation of different kinds of etch pits. The selective dissolution of (1 1 0), (1 1 0) and (1 0 0) planes of MMTC, CMTC and ZCTC with water and ethanol as etchants, suggests that the crystal growth is progressed with different growth pattern. The AFM study indicates that among the three crystals, CMTC has a smooth surface when compared with MMTC and ZCTC crystals. The data for average roughness (S_a), root mean square (S_q) value, ten-point height (S_z), surface skewness (S_{sk}) and surface kurtosis (S_{ku}) were estimated and compared for the three samples.

Acknowledgement

The authors are grateful to Department of Science and Technology (DST)-SERC, India for funding this project work (SR/S2/LOP-03/2007). The authors acknowledge Prof. Shi Feng Du and Prof. H. Chen, Institute of Physics, Chinese Academy of Sciences, Beijing 100 190, China for AFM facility and fruitful discussions.

References

[1] X.Q. Wang, D. Xu, M.K. Lu, D.R. Yuan, J. Huang, G.W. Lu, G.H. Zhang, S.Y. Guo, H.X. Ning, X.L. Duan, Y. Chen, Y.Q. Zhou, Opt. Mater. 23 (2003) 335.
[2] G. Zhou, W.-Y. Wong, Z. Lin, C. Ye, Angew. Chem. Int. Ed. 45 (2006) 6189.
[3] G. Zhou, W.-Y. Wong, S.-Y. Poon, C. Ye, Z. Lin, Adv. Funct. Mater. 19 (2009) 531.
[4] G.J. Zhou, W.Y. Wong, C. Ye, Z. Lin, Adv. Funct. Mater. 17 (2007) 963.
[5] Z. Yuan, C.D. Entwistle, J.C. Collings, D. Albesa-Jové, A.S. Batsanov, J.A.K. Howard, N.J. Taylor, H.M. Kaiser, D.E. Kaufmann, S.-Y. Poon, W.-Y. Wong, C. Jardin, S. Fathallah, A. Boucekkine, J.-F. Halet, T.B. Marder, Chem. Eur. J. 12 (2006) 2758.
[6] J.C. Collings, S.-Y. Poon, C. Le Droumaguet, M. Charlot, C. Katan, L.-O. Palsson, A. Beeby, J.A. Mosely, H.M. Kaiser, D. Kaufmann, W.-Y. Wong, M. Blanchard-Desce, T.B. Marder, Chem. Eur. J. 15 (2009) 198.
[7] H.S. Nalwa, Appl. Organomet. Chem. 5 (1991) 349.
[8] W.-Y. Wong, Coord. Chem. Rev. 249 (2005) 971.
[9] W.-Y. Wong, Cheuk-Lam Ho, Coord. Chem. Rev. 220 (2006) 2627.
[10] W.-Y. Wong, Cheuk-Lam Ho, Coord. Chem. Rev. 253 (2009) 1709.
[11] W.-Y. Wong, Coord. Chem. Rev. 251 (2007) 2400.
[12] W.-Y. Wong, Dalton Trans. (2007) 4495.
[13] W.-Y. Wong, Macromol. Chem. Phys. 209 (2008) 14.
[14] G.R. Whittell, I. Manners, Adv. Mater. 19 (2007) 3439.
[15] V. Petkov, Mater. Today 11 (2008) 28.
[16] P. Ginson Joseph, K. Rajarajan, M. Vimalan, S. Selvakumar, S.M. Ravi kumar, J. Madhavan, P. Sagayaraj, Mater. Res. Bull. 42 (2007) 2040.
[17] S. Selvakumar, J. Packiam Julius, S.A. Rajasekar, A. Ramanand, P. Sagayaraj, Mater. Chem. Phys. 89 (2005) 244.
[18] N. Zhang, M.H. Jiang, D.R. Yuan, D.R. Yuan, D. Xu, X.T. Tao, Z.S. Shao, J. Cryst. Growth 102 (1990) 581.
[19] X.Q. Wang, D. Xu, M.K. Lu, D.R. Yuan, J. Huang, S.G. Li, G.W. Lu, H.Q. Sun, S.Y. Guo, G.H. Zhang, X.L. Duan, H.Y. Liu, W.L. Liu, J. Cryst. Growth 247 (2003) 432.
[20] P. Ginson, J. Joseph, K. Philip, S.A. Rajarajan, A. Rajasekar, K. Joseph Arul Pragasam, S. Thamizharasan, M. Ravi Kumar, P. Sagayaraj, J. Cryst. Growth 296 (2006) 51.
[21] P. Ginson, K. Joseph, M. Raja Rajan, P.C. Vimalan, J. Thomas, S. Madhavan, M. Ravi Kumar, G. Gulam Mohamed, P. Mani, Sagayaraj, Cryst. Res. Technol. 42 (2007) 247.
[22] D. Yuan, Z. Zhong, M. Liu, D. Xu, Q. Fang, Y. Bing, S. Sun, M. Jiang, J. Cryst. Growth 186 (1998) 240.
[23] R.G. Pearson, J. Am. Chem. Soc. 85 (1963) 3533.
[24] C. Balarew, R. Duhlew, J. Solid State Chem. 55 (1984) 1.
[25] X.Q. Wang, D. Xu, M.K. Lo, D.R. Yuan, G.H. Zhang, F.Q.M.Q. Meng, S.Y. Guo, M. Zhou, J.R. Liu, X.R. Li, Cryst. Res. Technol. 36 (2001) 73.
[26] X.Q. Wang, D. Xu, M.K. Lu, D.R. Yuan, S.X. Xu, Mater. Res. Bull. 36 (2001) 879.
[27] Y.L. Geng, D. Xu, X.Q. Wang, D.Y. Pan, G.H. Zhang, G.W. Yu, J. Cryst. Growth 280 (2005) 226.
[28] M. Lizuka, T. Sudo, Z. Kristallogr. 126 (1968) 376.
[29] U. Von Hundelshausen, Phys. Lett. 34 (1971) 405.
[30] D. Yuan, D. Xu, M. Liu, F. Qi, W. Yu, W. Hou, Y. Bing, S. Sun, M. Jiang, Appl. Phys. Lett. 70 (5) (1997) 544.
[31] X.N. Jiang, D. Xu, D.L. Sun, D.R. Yuan, M.K. Lu, S.Y. Guo, G.H. Zhang, J. Cryst. Growth 234 (2002) 480.
[32] H. Nakatani, W.R. Bosenberg, L.K. Cheng, C.L. Tang, Appl. Phys. Lett. 53 (1988) 2587.
[33] J. Swain, S. Stokowski, D. Milan, F. Rainer, Appl. Phys. Lett. 40 (1982) 350.
[34] K. Sangwal, J. Servat, F. Sanz, J. Torrent Burgues, J. Cryst. Growth 180 (1997) 263.
[35] S. Manivannan, Dhanuskodi, S.K. Tiwari, J. Philip, J. Appl. Phys. B 90 (2008) 489.

[36] D.N. Nikogosyan, Nonlinear Optical Crystals: A Complete Survey, Springer, New York, 2005.
[37] V.G. Dmitriev, G.G. Gurzadyan, D.N. Nikogosyan, Handbook of Nonlinear Optical Crystals, 3rd edn., Springer, Berlin, 1999.
[38] V. Venkataramanan, C.K. Subramanian, H.L. Bhat, J. Appl. Phys. 77 (1995) 6049.
[39] B.C. Stuart, M.D. Feit, Rubenchick, B.W. Shore, M.D. Perry, Phys. Rev. Lett. 74 (1995) 2248.
[40] M. Raposo, Q. Ferreia, P.A. Ribeiro, Modern research and educational topics in microscopy, in: A. Mendz-Vilas, J. Diaz (Eds.), Micorscopic Book Series, Formatex, 2007, p. 758.